Xinru Li[1] and Simon Donner[1]

1. Department of Geography, University of British Columbia, Vancouver, B.C., Canada

Corresponding author: Xinru Li (`xinrulicco@gmail.com`)

Key points

- There are considerable regional biases in the thermal properties of warm-season marine heatwave in three CMIP6 models

- Models biases in the thermal properties are likely caused by different model representations of related atmospheric and oceanic processes

- In contrast to duration, accumulated heat stress and peak intensity, heating rate and "priming" duration are projected to decline by 2100

Abstract

Marine heatwaves in the summertime when temperatures may exceed organisms' thermal thresholds ("warm-season MHWs") have huge impacts on the health and function of ecosystems like kelp forests and coral reefs. While previous studies showed that MHWs are likely to become more frequent and severe under future climate change, there has been less analysis of the thermal properties of warm-season MHWs or on the effects of climate model biases on these projections. In this study, we examine CMIP6 model ability to simulate five key thermal properties of warm-season MHWs, and evaluate the global pattern of future projections for coral reef and kelp systems. The results show that the duration, accumulated heat stress and peak intensity are projected to increase by > 60 day, $160\ °C \cdot day$ and $1\ °C$, respectively, across most of the ocean by the end of 21st century. In contrast, the duration of "priming" (a period of sub-lethal heat stress prior to MHW development) is projected to decrease by > 30 day in the tropics, potentially reducing organisms' ability to acclimate to heat stress. The projected increases in the MHW duration and accumulated heat stress in some coral reef and kelp forest locations, however, are likely overestimated due to model limitations in simulating surface winds, deep convections and some other processes that influence MHW evolution. The findings point to the processes to target in model development and regional biases to be considered when projecting the impacts of MHWs on marine ecosystems.

Plain Language Summary

Periods of extremely high ocean temperatures that persist for days to months, known as Marine Heatwaves (MHWs), can cause the loss of marine life and impact coastal communities and economies. Climate change is expected to drive substantial increases in the length, strength and frequency of MHWs this century. There has been less analysis, however, of the characteristics of individual MHWs, like the rate at which they develop. In this research, we examine how well climate models can simulate these characteristics and the implication for

future projections. We find considerable biases in the simulation of some key MHW characteristics in parts of the ocean due to model limitations in capturing physical processes like surface winds along the equator. Most MHW characteristics like duration and total heat stress are projected to increase sharply this century, particularly for coral reefs and kelp forests, although the increases in some regions are likely overestimated due to model biases. Conversely, we project decreases in "priming" – periods of sub-lethal heat stress that help marine life prepare for heat waves. These findings identify regional errors to consider when interpreting MHW projections and can help researchers identify areas for improving model performance.

1. Introduction

Over the past few decades, marine heatwaves (MHWs) have become longer, stronger and more frequent (Frölicher et al., 2018; X. Li & Donner, n.d.; Oliver et al., 2018). These periods of anomalously high sea surface temperatures (SSTs) have severely affected marine ecosystems including changes in species distributions, mass mortality, loss of biomass, degradation of ecosystem function and decline in ecosystem services (Arias-Ortiz et al., 2018; Cheung et al., 2021; Smale et al., 2019). MHWs during the summer or warm-season, when temperatures are more likely to exceed organisms' upper thermal tolerance, are a particular threat to habitat-forming systems in which the foundational species are vulnerable to heat stress. Warmwater coral reefs are susceptible to heat stress of as little as 1-2 °C above long-term average summer temperature, which can interrupt the symbiont relationship between coral and microalgae living in coral tissue, leading to the phenomenon known as coral bleaching. For example, more than 75% of warmwater coral reefs experienced some bleaching during 2014 and 2017, which caused mass loss of living coral and cascading effects on reef ecosystems (Hughes et al., 2017; W. J. Skirving et al., 2019; Sully et al., 2019). Kelp forests are also severely threatened by MHWs, which can cause mass mortality, changes in the food web and phase shifts to urchin-dominated systems (Arafeh-Dalmau et al., 2019; Filbee-Dexter et al., 2020; Rogers-Bennett & Catton, 2019; Smale, 2020).

It has been well documented that MHWs are likely to become more frequent, intensive and longer-lasting under climate change throughout the 21st century (Frölicher et al., 2018; Oliver et al., 2019). Most studies of the projected impacts of MHWs on marine ecosystems have focused on the frequency and intensity of MHWs, and not considered other properties which can affect marine ecosystems and organisms. For example, most projections of the effects of MHWs on coral reefs employ accumulated heat stress, a metric measuring the combination of duration and magnitude of heat stress as the indicator of coral bleaching conditions (Skirving et al., 2020), while the rate of heat stress development, which can influence mortality of coral reef fish (Genin et al., 2020), has not been assessed. In addition, there has been limited analysis of the duration of pre-MHW "priming" – a period of sub-lethal heat stress in advance of warm-season MHW development which can influence the response of corals and other ma-

2

rine organisms to severe heat stress (Ainsworth et al., 2016; Hilker et al., 2016). Evaluating these fine-scale MHW properties could help better understand and project how MHWs affect marine ecosystems.

Projections of MHW properties and their effects on marine ecosystems depend on the ability of models to represent the atmospheric and oceanic processes that influence MHW development and dissolution. While previous studies evaluated MHW projections with outputs from ensembles of General Circulation Models (GCMs) and Earth System Models (Frölicher et al., 2018; Oliver et al., 2019; Plecha et al., 2021), there has been less analysis of model biases in simulating the baseline characteristics of MHWs, and how such biases may affect future projections. Challenges in simulating air-sea interactions, the periodicity and diversity of El Niño / Southern Oscillation (ENSO) dynamics, and other key climate phenomena due to limits of model resolution and other factors can lead to regional biases in mean and seasonal SST (Brown et al., 2020; Guo et al., 2022; Jiang et al., 2021; G. Li & Xie, 2012; Toniazzo & Woolnough, 2014; Wang et al., 2014). These model biases could reduce accuracy of the projected MHW thermal properties and their ecological impacts (Hoeke et al., 2011; van Hooidonk & Huber, 2012). Though a large ensemble of models might present a more accurate representation of mean SSTs (Frölicher et al., 2016; Weigel et al., 2010), some of the process-derived biases in individual models cannot cancel each other out (Frölicher et al., 2018; Oliver et al., 2019). Evaluating the model biases can indicate key processes to target in model development, and identify biases to be considered when projecting local or regional ecological impacts of warm-season MHWs.

In this study, we aim to improve our understanding of the future thermal properties of warm-season MHWs by assessing their projected changes in light of historical model biases, using three CMIP6 models. First, we compare historical model simulations against observations to identify the regional biases in warm-season MHW properties, including the duration, peak intensity, accumulated heat stress, heating rate and duration of the priming period. Second, we evaluate future projections of warm-season MHW properties under three Shared Socio-Economic Pathways (SSPs). Third, we examine the MHW projections for coral reef and kelp systems worldwide considering the role of the regional model biases. We then discuss the possible physical drivers of regional model biases and disagreement between model projections.

2. Methods

2.1 Definition of warm-season MHW and the metrics characterizing its thermal properties

A warm-season MHW is defined here as a period of positive anomalies of daily SSTs or HotSpots (HS), relative to the thermal threshold known as the Maximum Monthly Mean (MMM), that represents the climatological warm-season SST and is commonly used for predicting coral bleaching. The MMM in each grid cell is calculated as the maximum from a 1985-2014 monthly mean SST

3

climatology. To test the effects of theoretical acclimation or adaptation to warming by marine ecosystems, we repeat the analysis using a rolling climatology (Logan et al., 2014), in which the MMM is calculated based on the previous sixty year period.

We define a set of metrics for characterizing warm-season MHWs in terms of magnitude, duration, accumulated heat stress and heating rate (Table 1), following Li & Donner (2022). The duration of heat stress is described by D_c, the duration of continuous positive HS, and D_{tot}, the total number of days with positive HS. The "priming" period (D_p), a period of sub-lethal heat stress that might train marine organisms' thermal tolerance (Hilker et al., 2016), is computed as the number of days from the first positive HS in a year to the onset of D_c. The accumulated heat stress over the continuous period (D_c) and for the annual total (D_{tot}) are described by the metrics A_c and A_{tot}, respectively. As the total number of positive HS days (D_{tot}) is longer than or at minimum equal to the duration of continuous heat stress (D_c), the accumulated heat stress over all HS days is greater than or at minimum equal to that over the period of continuous heat stress. Finally, the heating rate (HR_c) is the rate of warming from the start of the continuous heat stress period to the date of peak HS.

Variable	Description	
HotSpot (°C)	HS_{MMM}	Daily HotSpot in that grid cell, using MMM baseline
	HS_{peak}	Maximum HS value that year
Duration (day)	D_c	Duration of continuous positive HotSpot, based on the period that includes the maximum annual HotSpot
	D_{tot}	Total number of days with positive HotSpot
	D_p	Number of days between the first positive HotSpot and onset of a continuous positive HotSpot period (i.e., D_c), referring to the "conditioning or priming period"

Variable	Description	
Accumulated heat stress (°C · day)	A_c	Accumulated sum of heat stress during the continuous positive HotSpot period, based on the time period used for D_c
	A_{tot}	Accumulated sum of all HotSpot that year
Heating rate (°C · day^{-1})	HR_c	Rate of SST increase from the start of the D_c period to the date of HS_{peak}

Table 1. Metrics measuring the thermal properties of warm-season MHWs.

All of the annual warm-season MHW properties are defined for a given heat stress year (HSY). The HSY starts from a month in the climatological cold season in the given grid cell (Li & Donner, 2022). This spatially varying definition of the HSY is necessary because the warm season in parts of the ocean overlaps across two calendar years. In the remainder of the manuscript, we use the word "year" instead of HSY for clarity, and label them according to the first calendar year of a HSY. For example, the last year of the historical heat stress analysis refers to HSY 2013, including data from the calendar years 2013 and 2014.

To test the effects of theoretical acclimation or adaptation to warming by marine ecosystems for the end of the century, we repeat the analysis using the end point of rolling climatology (Logan et al., 2014), in which the MMM is calculated over the 2041-2100 period.

2.2 Coral reef and kelp forests distribution

Projected changes of warm-season MHW properties are also specifically assessed over the global region of coral reef and kelp systems according to the high resolution global maps of warmwater corals (UNEP, 2010) and the Laminarian kelp biome (Jayathilake and Costello 2020). The maps are converted to global 1° x 1° latitude-longitude grids using ArcGIS for consistency with the grid of model outputs.

3 Sea surface temperature datasets

We use 1° x 1° latitude-longitude global daily SST outputs from the simulations of historical (1985-2014) and future climate (2015-2100) in the Coupled Model Intercomparison Project Phase 6 (CMIP6, Eyring et al. 2016). All the simulation outputs are from the first ensemble member (r1i1p1) of three models: GFDL-ESM4 (Dunne et al., 2020), MRI-ESM2 (Yukimoto et al., 2019) and CESM2-WACCM (Danabasoglu et al., 2020). These three models are employed

because i) they have low, medium and high climate sensitivities relative to the range of values in the CMIP6 ensemble (2.7K, 3.4K and 4.8K, respectively); ii) they have relatively strong performance in simulating key natural modes of climate variability (e.g., ENSO, Dunne et al. 2020; Beobide-Arsuaga et al. 2021; Danabasoglu et al. 2020), which is critical to simulating warm-season MHW frequency and severity (Sen Gupta et al., 2020; Holbrook et al., 2019; Oliver et al., 2018). The future projections are examined for three future scenarios, SSP 1-2.6, SSP 2-4.5 and SSP 3-7.0, used in the CMIP6 that represent a low, medium and high level of radiative forcing in the range of the future emission pathways (O'Neill et al., 2016). Note that most of the CMIP6 model simulation outputs are available for download with the original native tripolar grid in unit of kilometer. For the consistency, we regridded the CESM2-WACCM outputs using the same 1st order conservative algorithm that data centers used for the regridded GFDL-ESM4 and MRI-ESM2 outputs (Jones 1999).

We use 0.05° x 0.05° latitude-longitude global daily satellite-derived SST dataset CoralTemp v3.1 from the National Oceanic and Atmospheric Association (NOAA) Coral Reef Watch (CRW) program (W. Skirving et al., 2020), to contrast simulations and observations for the 1985-2014 historical period. For the consistency of the spatial resolution between the observed and simulated SST data, we regridded the observed SST datasets to 1° by 1° using the 1st order conservative algorithm (i.e., a common method used for upscaling dataset resolution; Jones 1999).

4. Results

4.1 Evaluation of model biases in the thermal properties of warm-season MHW over the historical (1985-2014) period
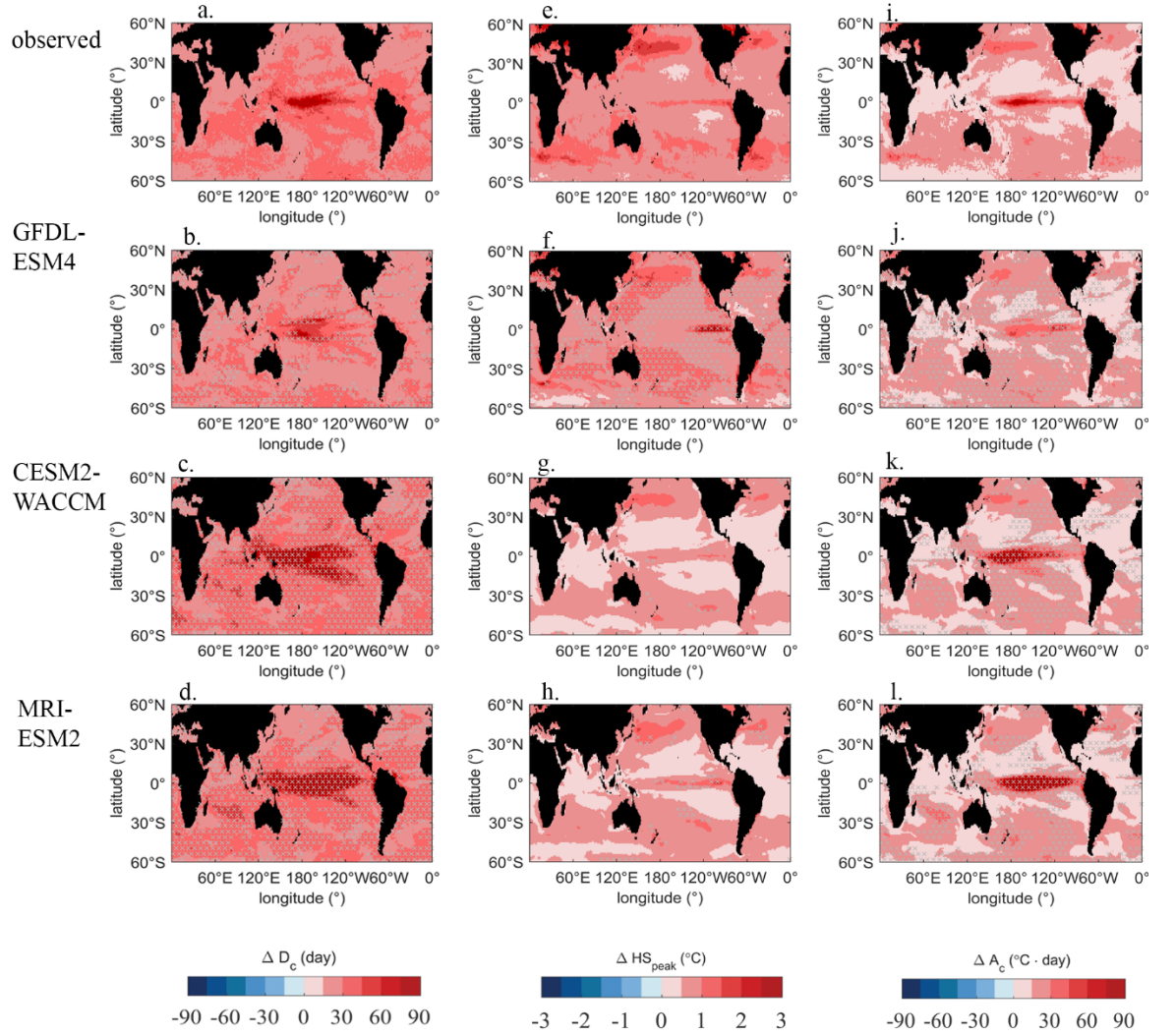
Figure 1. Mean warm-season MHW properties over the 1985-2014 period. (a-d) the mean duration of the continuous warm-season MHW (D_c, day); (e-h) the mean annual peak HS (HS_{peak}, °C); (i-l) the mean accumulated heat stress of the continuous warm-season MHW (A_c, °C · day). The mean states from the first to last rows correspond to the properties observed and simulated by GFDL-ESM4, CESM2-WACCM and MRI-ESM2, respectively.
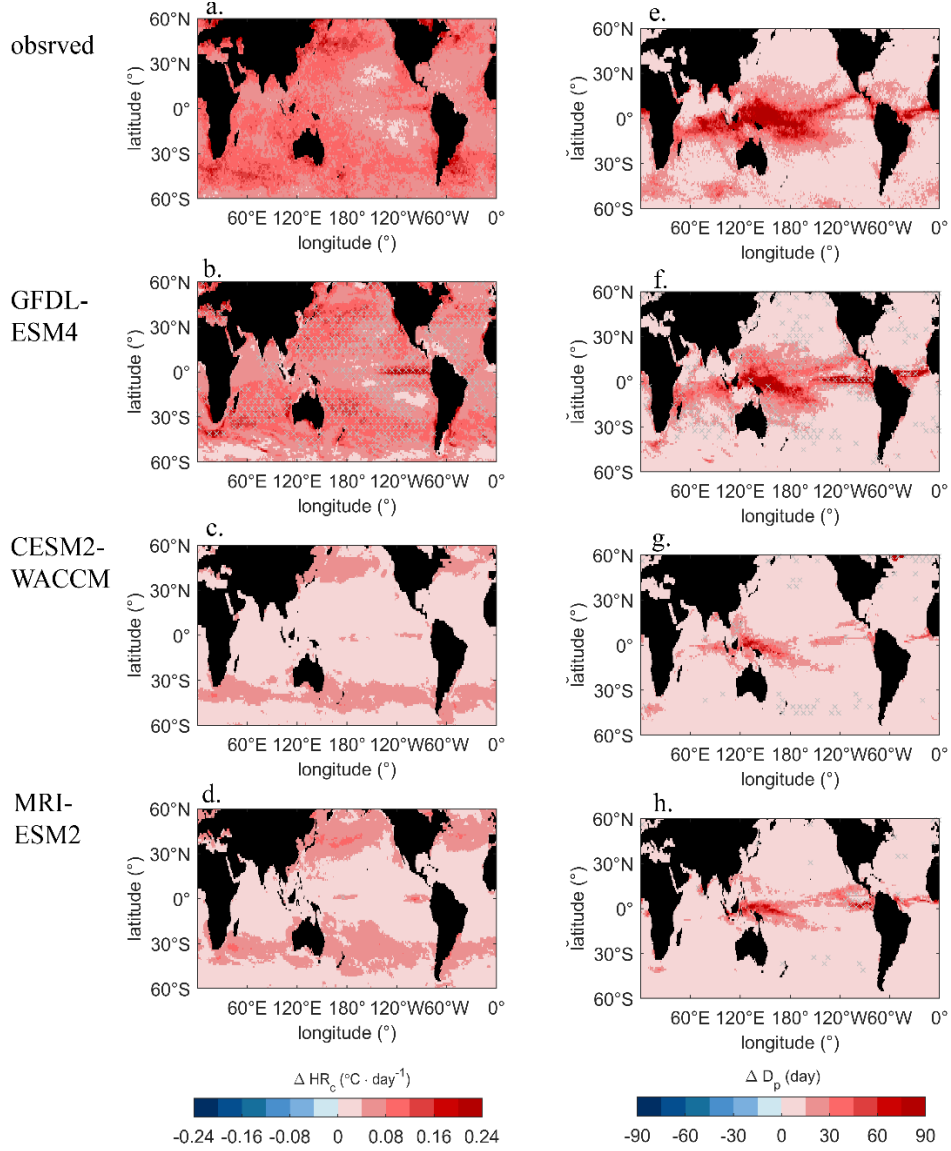
Figure 2. Mean warm-season MHW properties over the 1985-2014 period. (a-d) the heating rate (HR_c, $°C \cdot day^{-1}$), measured from the onset of a continuous event to annual peak HS; (e-h) the priming period (D_p, day), measured as the number of days between the first HS of a year and the start of the continuous MHW. The mean states from the first to last rows correspond to the properties observed and simulated by GFDL-ESM4, CESM2-WACCM and MRI-ESM2, respectively.

The mean warm-season MHW properties, including the duration (D_c), accumu-

lated heat stress (A_c), annual peak HS (HS_{peak}), heating rate (HR_c) and "priming" period (D_p), simulated by GFDL-ESM4 generally show smaller magnitudes of model bias versus observations than CESM2-WACCM and MRI-ESM2 (Figure 1, 2, S1, 2). The spatial pattern of the biases in these thermal properties is similar between CESM2-WACCM and MRI-ESM2, and different from that of GFDL-ESM4 (Figure S1, 2).

In CESM2-WACCM and MRI-ESM2, D_c and A_c are overestimated by higher magnitudes (i.e., up to 60 day and 60 °C · day in the tropical Pacific) across more of the ocean than those in GFDL-ESM4 (Figure 1a, 1c, 1d, S1a-c). The global pattern of biases is similar for the accumulated heat stress (A_c) to that for D_c in the three models (Figure 1i-l, S1g-i), which suggests a larger contribution of D_c than HS_{peak} to A_c. The longer duration and the associated greater accumulated heat stress are related to damped daily SST variability in the warm-season in CESM2-WACCM and MRI-ESM2 that could result in smoother HS time series (Figure S3). The annual total heat stress days (D_{tot}) and accumulated total heat stress (A_{tot}), versions of the duration and accumulated heat stress metrics used in previous studies (e.g., Frölicher et al. 2018; Oliver et al. 2018), show similar spatial distribution of model biases to those of D_c and A_c in each of the three models (Figure S4).

Unlike the duration and accumulated heat stress, the maximum intensity (HS_{peak}) and heating rate (HR_c) are overestimated by GFDL-ESM4, and underestimated by CESM2-WACCM and MRI-ESM2 across most of the ocean (Figure 1, 2, S1, S2). GFDL-ESM4 overestimates HS_{peak} up to 0.2-0.8 °C across most of the low- to mid- latitudes of the ocean, particularly in the eastern tropical Pacific (Figure 2b, S2a). In contrast, HS_{peak} is mostly underestimated in CESM2-WACCM and MRI-ESM2, with the largest underestimates up to 1.2 °C in the western boundary current and extension regions at high latitudes (Figure 1g-h, S1e-f), where model underestimates of interannual variability of the warmest month SSTs contributes to the negative biases in HS_{peak} (Figure S5). Smaller underestimates of up to 0.6 °C also show in these regions with GFDL-ESM4 output (Figure S1d).

For heating rate (HR_c), the spatial bias patterns in the three models appear driven by that of HS_{peak}. In GFDL-ESM4, a large fraction of the ocean shows great overestimates in the eastern equatorial Pacific (up to 0.18 °C · day^{-1}, i.e., simulated HR_c up to double its observed historical level), as the positive biases in HS_{peak} and the negative biases in D_c both contribute to the overestimates (Figure 1a-b, 1e-f, 2a-b, S1a, 1d, 2a). In contrast, large underestimates of HR_c, above 0.12 °C · day^{-1}, occur across most of the ocean in ESM2-WACCM and MRI-ESM2, due to the negative biases in HS_{peak} and the positive biases in D_c (Figure 1e-h, 2a-d, S1e-f, S2b-c).

The priming period (D_p) is mostly underestimated, particularly in the western to central tropics with the largest underestimates up to 90 day (Figure 2e-h, S2d-f). The negative biases in D_p are largely driven by the positive biases in D_c,

as short periods of continuous heat stress combined into one longer continuous period. This is also reflected in the larger negative biases for D_p in CESM2-WACCM and MRI-ESM2, as the models show larger positive biases for D_c. (Figure S1b-c, S2e-f). Conversely, there are large overestimates, up to 90 day in GFDL-ESM4 and 60 day in MRI-ESM2, over the eastern equatorial Pacific where the model overestimated variability of daily warm-season SSTs contribute to a higher chance of occurrence of longer D_p (Figure 2e-h, S2d-f, S3).

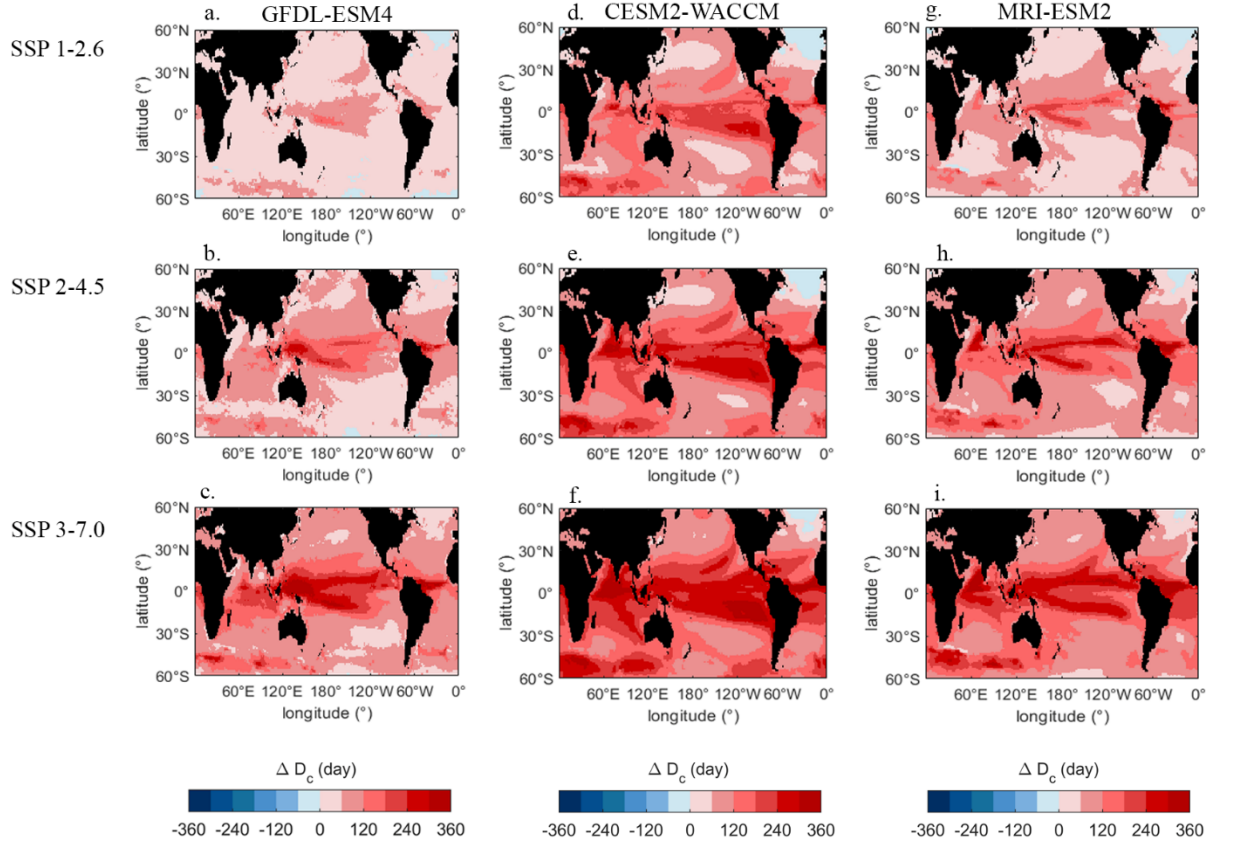4.2 Evaluation of future projected changes in warm-season MHW properties

Figure 3. Mean projected changes of the duration of continuous warm-season MHW (D_c, day) by the end of 21st century (2071-2100) relative to the historical period (1985-2014). The mean states from the first to last columns are simulations by GFDL-ESM4, CESM2-WACCM and MRI-ESM2 and those from the first to last rows refer to the simulations under SSP1-2.6, SSP2-4.5, SSP3-7.0 scenarios, respectively.
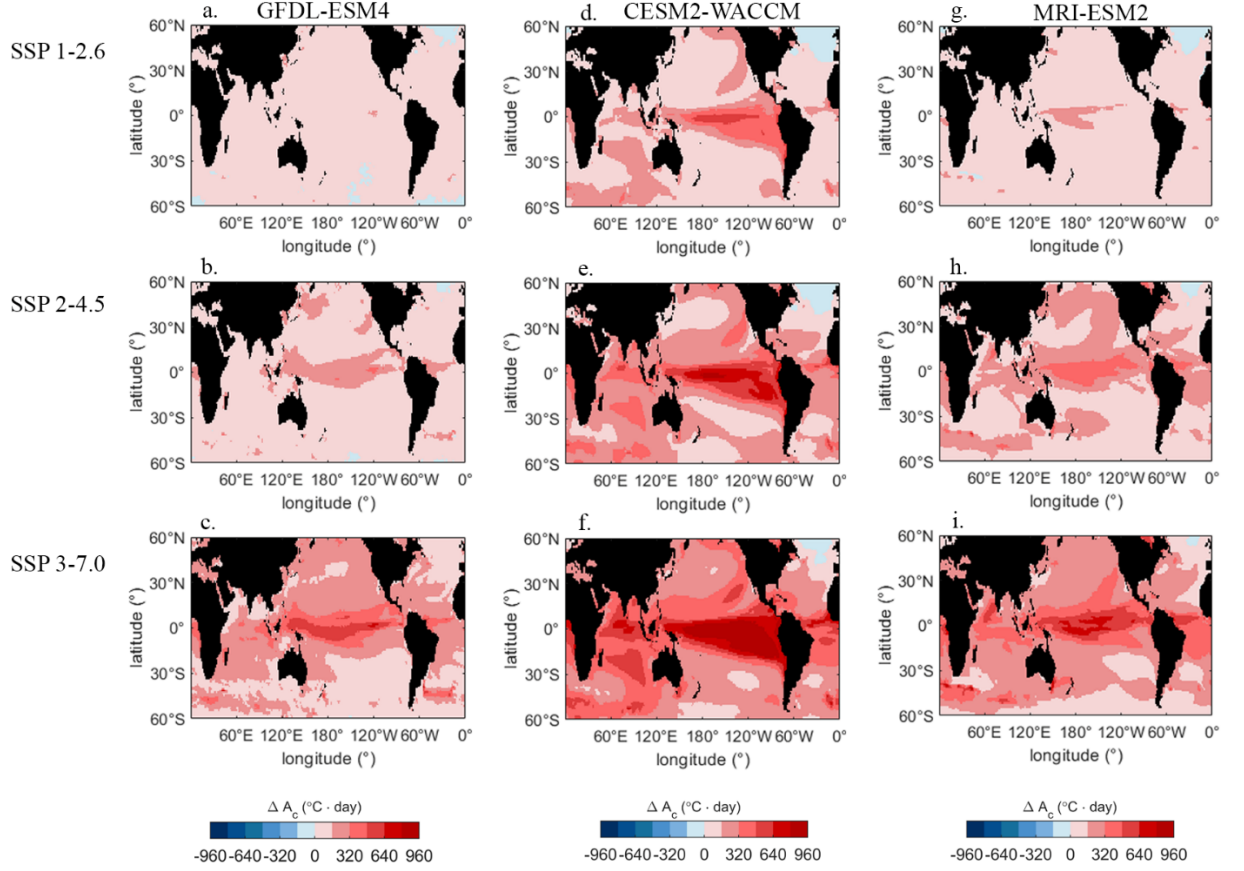
Figure 4. Mean projected changes of the accumulated heat stress of the continuous warm-season MHW (A_c, °C · day) by the end of 21st century (2071-2100) relative to the historical period (1985-2014). The mean states from the first to last columns are simulations by GFDL-ESM4, CESM2-WACCM and MRI-ESM2 and those from the first to last rows refer to the simulations under SSP1-2.6, SSP2-4.5, SSP3-7.0 scenarios, respectively.
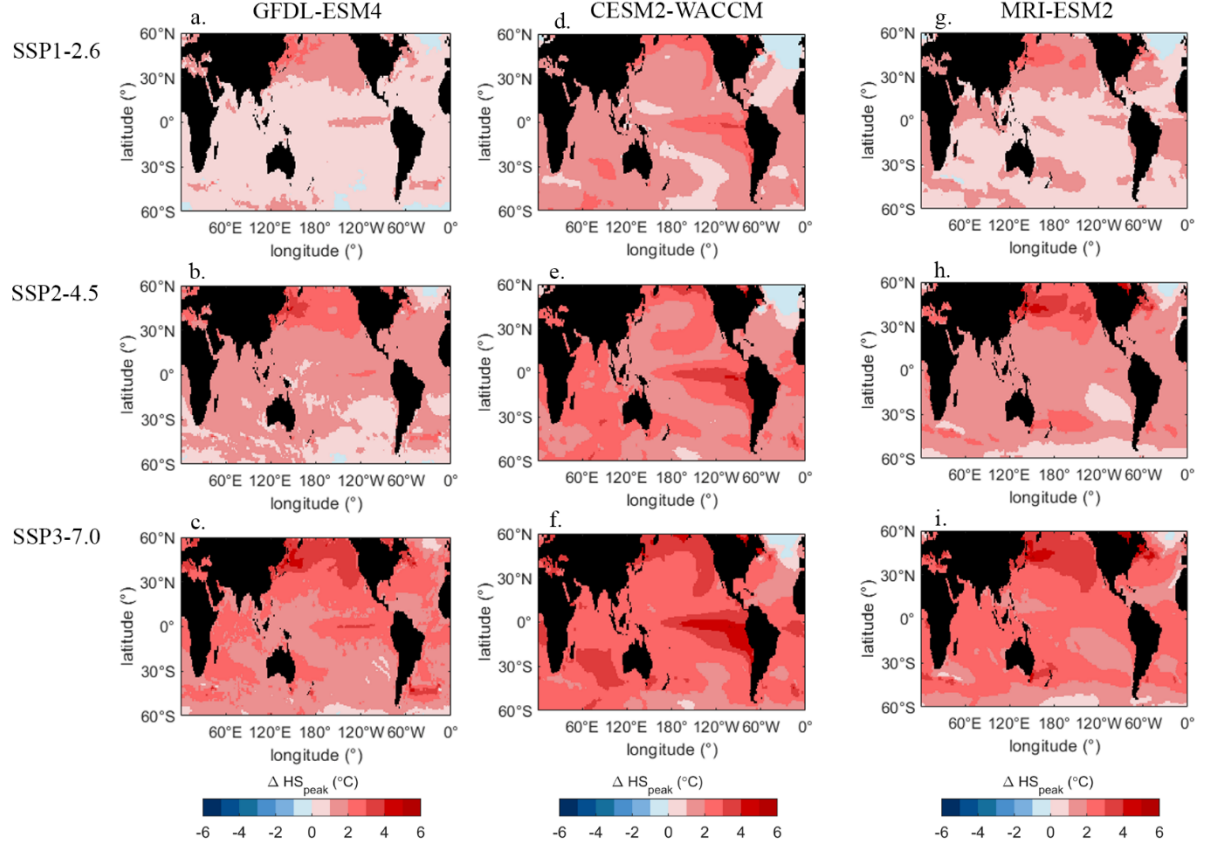
Figure 5. Mean projected changes of annual peak HS (HS$_{peak}$, °C) by the end of 21st century (2071-2100) relative to the historical period (1985-2014). The mean states from the first to last columns are simulations by GFDL-ESM4, CESM2-WACCM and MRI-ESM2 and those from the first to last rows refer to the simulations under SSP1-2.6, SSP2-4.5, SSP3-7.0 scenarios, respectively.

The duration (D$_c$), peak intensity (HS$_{peak}$) and accumulated heat stress (A$_c$) of warm-season MHWs are projected to increase across most of ocean, except the high latitudes of the North Atlantic, over the course of the 21st century according to all three models (Figure 3-5). The heating rate (HR$_c$) and priming period (D$_p$) are projected to decrease in some parts of ocean, especially with GFDL-ESM4 (Figure 6-7). The magnitude of the projected changes in these thermal properties is shaped by the models' climate sensitivities, with the highest projected changes in CESM2-WACCM (4.8K) followed by MRI-ESM2 (3.4K) and GFDL-ESM4 (2.7 K). The magnitude of these projected changes track that of surface ocean warming under different SSP scenarios; the changes are similar across all scenarios by mid-century, and greatest in the scenario with highest radiative forcing (SSP3-7.0) by end-century (also shown in Oliver et al., 2019; Figure 3-7, S6-10).

The largest increases of D_c occur in the tropical regions and the high latitudes of the Southern Hemisphere in all three models under SSP3-7.0 (Figure 3). For example, D_c is projected to increase by >300 day in GFDL-ESM4 in the western equatorial Pacific and south of southern Africa, implying a near-permanent warm-season MHW state. The limited seasonality in these regions implies that even a small increase in SST trend can lead to a sharp increase in the duration of heat stress, as SST is close to the climatological maximum throughout the year. The greatest model disagreement in duration occurs in the regions where there is also large disagreement in the mean values during the historical period (Figure 3, S1a-c). For example, the increases projected by CESM2-WACCM is up to 240 day longer than those projected by GFDL-ESM4 in the eastern tropical Pacific (Figure 3).

The accumulated heat stress shows similar global pattern to that of the equivalent duration variable (Figure 3, 4). The largest increases of A_c in GFDL-ESM4 are up to 320, 480 and 640 °C · day under SSP1-2.6, 2-4.5 and 3-7.0, respectively, which are substantially greater than what are currently classified as severe warm-season MHWs for coral reefs (e.g., a Level 2 Bleaching Alert from NOAA Coral Reef Watch occurs at the equivalent of 56 °C · day). As with D_c, there are disagreements among the models across the tropical Pacific with the highest climate sensitivity model CESM2-WACCM projecting increases of 480 °C · day greater than GFDL-ESM4 under SSP3-7.0 (Figure 3, 4). The largest increases of HS_{peak} with changes >5 °C are projected to occur in the high latitudes of the Northern Hemisphere in all three models, particularly in the subpolar gyre in Pacific (Figure 5). The projected changes of HS_{peak} in the tropical eastern Pacific are distinct among the models; for example, HS_{peak} is projected to increase by 2 °C more in CESM2-WACCM than in the other two models under SSP3-7.0 (Figure 5).
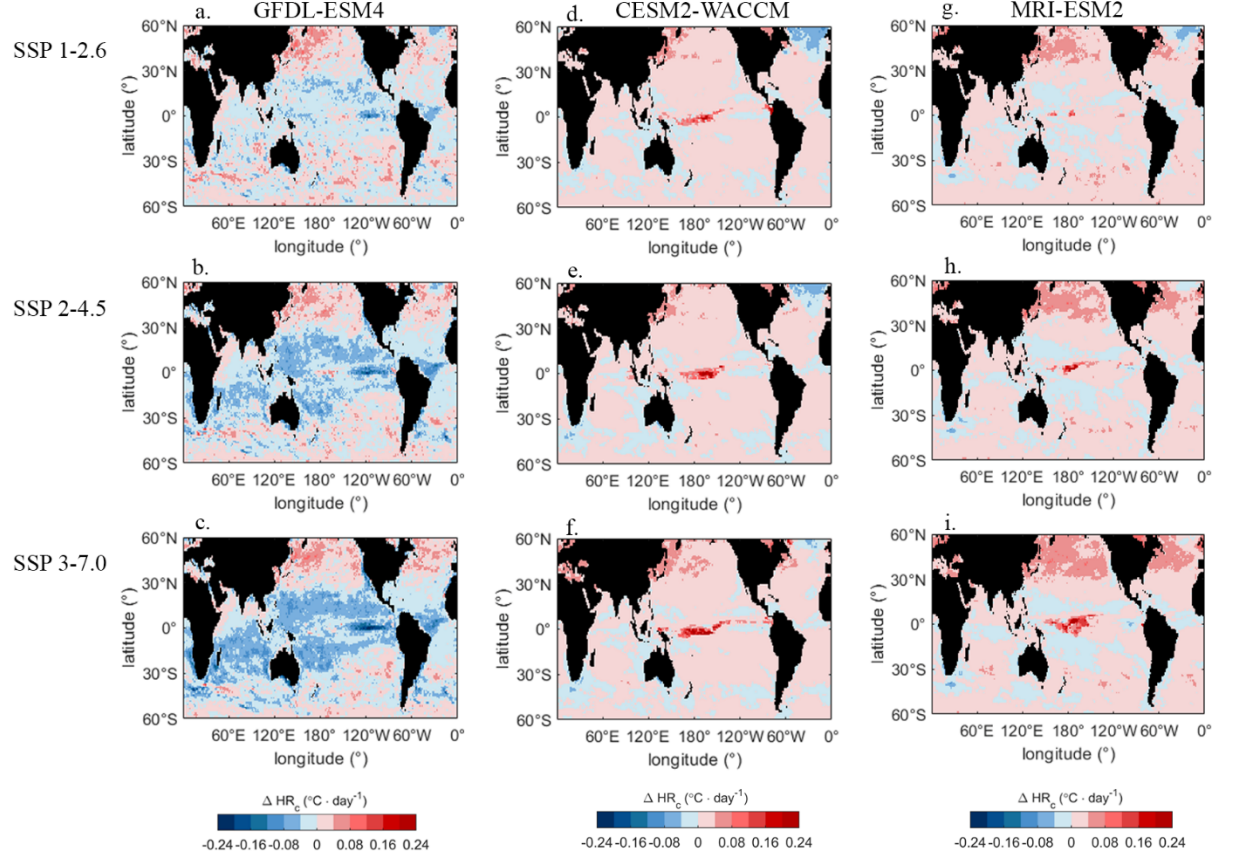
Figure 6. Mean projected changes of the heating rate (HR$_c$, $^{\circ}$C · day^{-1}), measured from the onset of a continuous event to annual peak HS, by the end of 21st century (2071-2100) relative to the historical period (1985-2014). The mean states from the first to last columns are simulations by GFDL-ESM4, CESM2-WACCM and MRI-ESM2 and those from the first to last rows refer to the simulations under SSP1-2.6, SSP2-4.5, SSP3-7.0 scenarios, respectively.
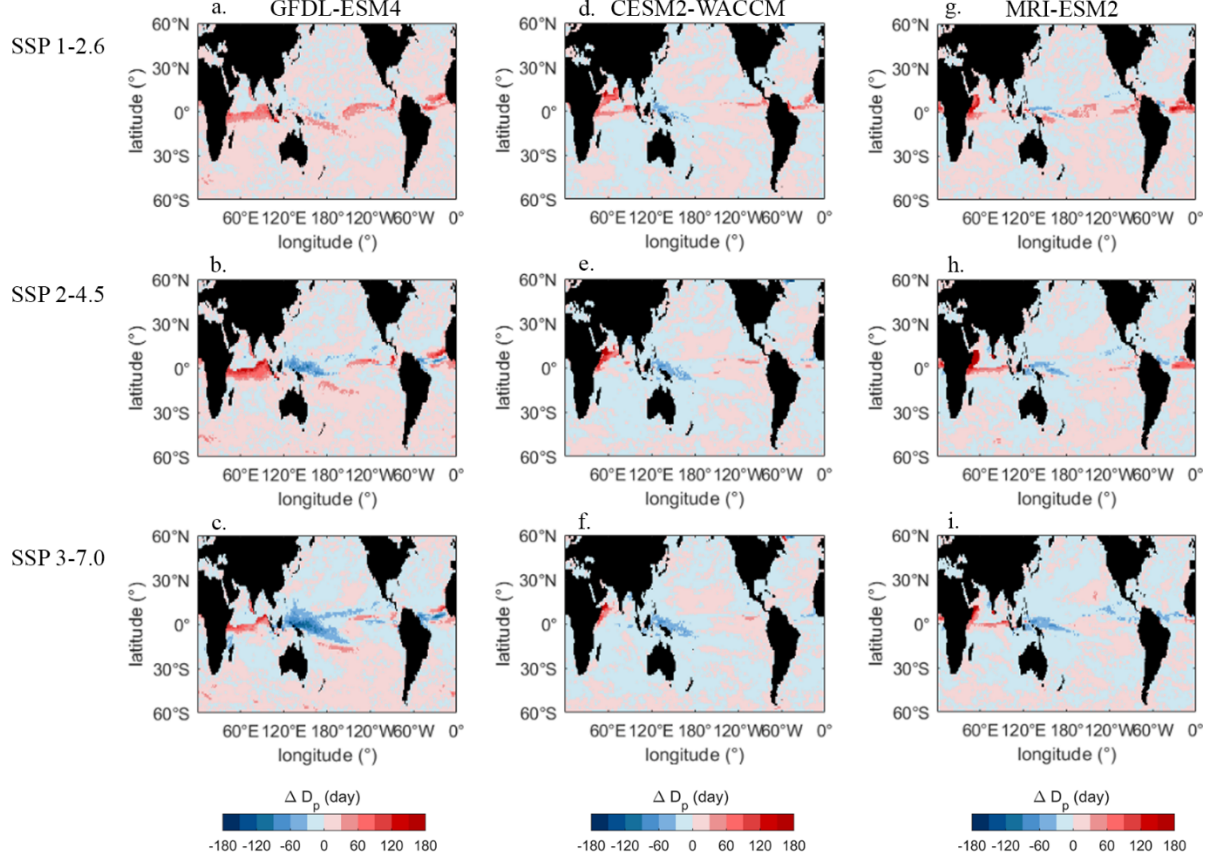
14

Figure 7. Mean projected changes in the priming period (D_p, day), measured as the number of days between the first HS of a year and the start of the continuous MHW, by the end of 21st century (2071-2100) relative to the historical period (1985-2014). The mean states from the first to last columns are simulations by GFDL-ESM4, CESM2-WACCM and MRI-ESM2 and those from the first to last rows refer to the simulations under SSP1-2.6, SSP2-4.5, SSP3-7.0 scenarios, respectively.

Unlike the duration, peak intensity and accumulated heat stress, a larger fraction of the ocean is projected to experience decreases in the heating rate (HR_c) and priming period (D_p), mostly in the tropics and subtropics (Figure 3-7). While most of the decreases in HR_c are small ($< 0.04\,°C \cdot day^{-1}$), the decreases in the subtropical Pacific in GFDL-ESM4 under SSP3-7.0 are up to $0.20\,°C \cdot day^{-1}$, which is roughly twice the mean heating rate in the historical period (Figure 2a, 6c). The declines of HR_c correspond with the greater rate of increase in D_c relative to that in HS_{peak}. In all three models, the duration of priming period is projected to decrease in the western tropical Pacific, in conjunction with the increases in D_c or the duration of continuous heat stress (Figure 3, 7). In

15

GFDL-ESM4, the largest decreases are as high as 150 day and approximately 60 day larger than with the other two models. In contrast, there are also increases in D_p with most below 30 day, although several large increases in D_p occur in the equatorial Indian and Atlantic Ocean in each of the three models (e.g., the increase >150 day under SSP3-7.0). These cases involve a long D_p followed by a short and mild MHW event, which does not fit the definition of priming in that a real priming period needs to occur prior to severe MHW event (Figure 7).

4.3 Projected changes in warm-season MHW properties over global areas of coral reef and kelp systems, and role of model biases
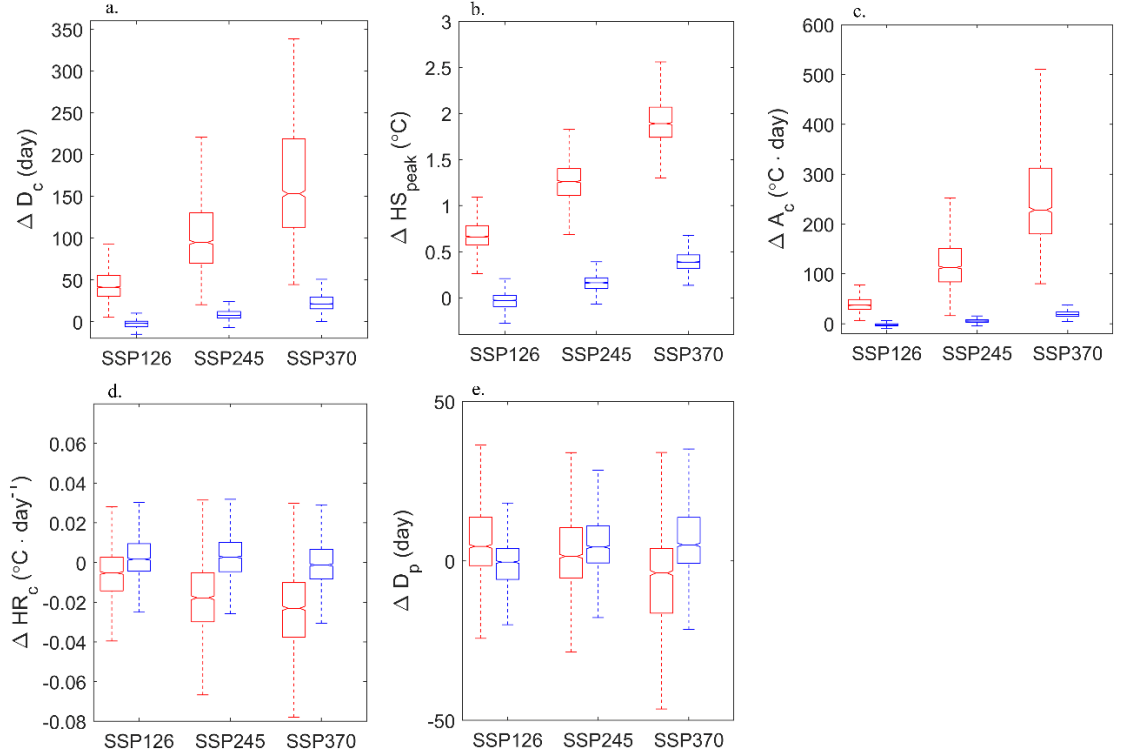

Figure 8. Mean projected changes of the warm-season MHW properties in coral reef cells by the end of 21st century (2071-2100) relative to the historical period (1985-2014) in GFDL-ESM4. a. the continuous warm-season MHW (D_c, day), b. the annual peak HS (HS_{peak}, °C), c. the accumulated heat stress over the continuous period (A_c, °C · day), d. the heating rate (HR_c, °C · day^{-1}), e. the priming period duration (D_p, day). The boxes in red are the thermal properties calculated based on the MMM threshold. The boxes in blue are the thermal properties calculated based on the rolling MMM over a climatological period from 2041 to 2100.
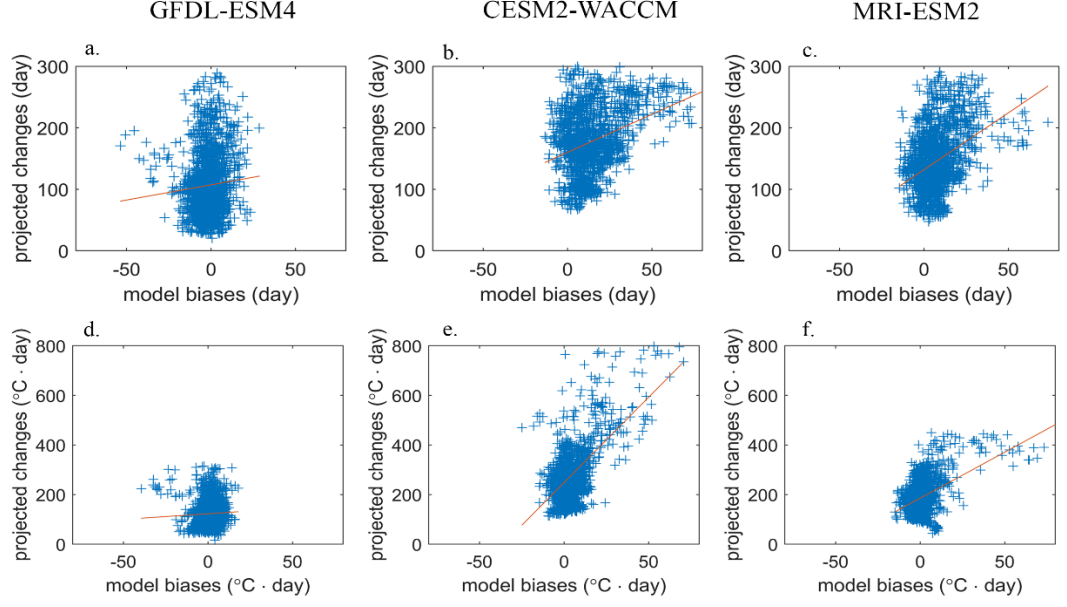
16

Figure 9. Historical model biases in warm-season MHW properties vs. the projected future changes over the global cells of coral reefs under SSP2-4.5 by the end of 21st century for the a.-c. the continuous warm-season MHW (D_c, day), d.-f. the accumulated heat stress over the continuous period (A_c, °C · day).
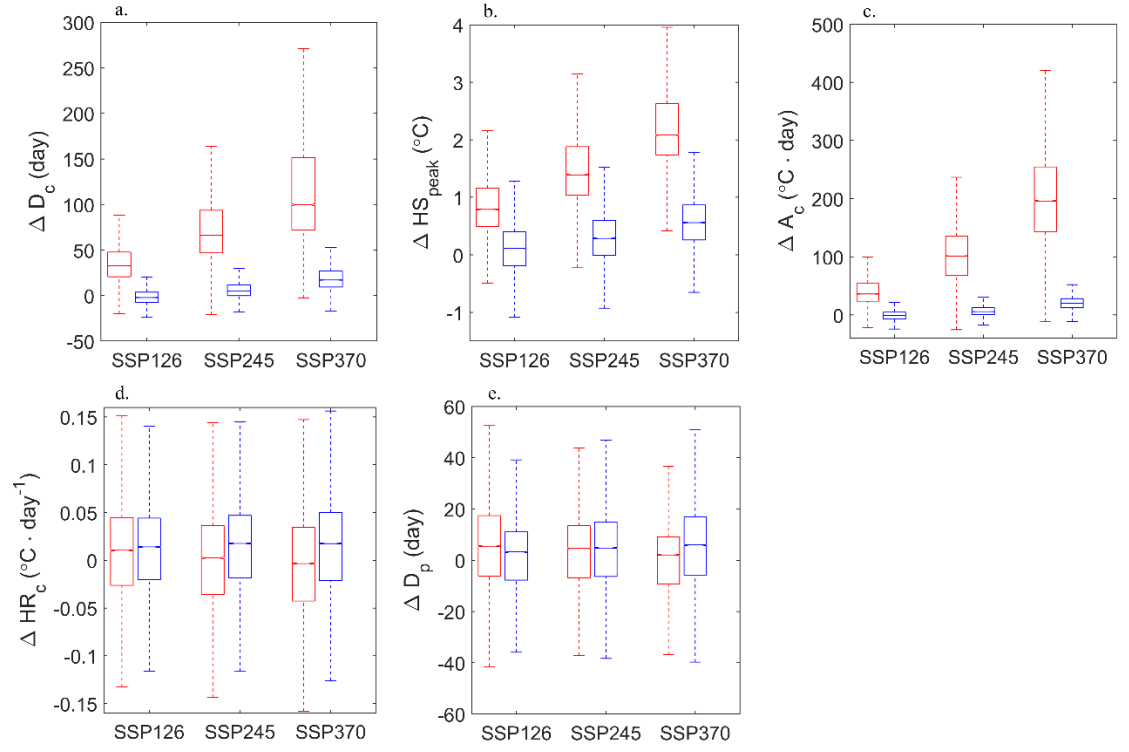
Figure 10. Mean projection changes of the warm-season MHW properties in kelp cells by the end of 21st century (2071-2100) relative to the historical period (1985-2014) by GFDL-ESM4 as in Figure 8, a. the continuous duration (D_c, day), b. the annual peak HS (HS_{peak}, °C), c. the accumulated heat stress over the continuous period (A_c, °C · day), d. the heating rate (HR_c, °C · day^{-1}), e. the duration of priming period (D_p, day).
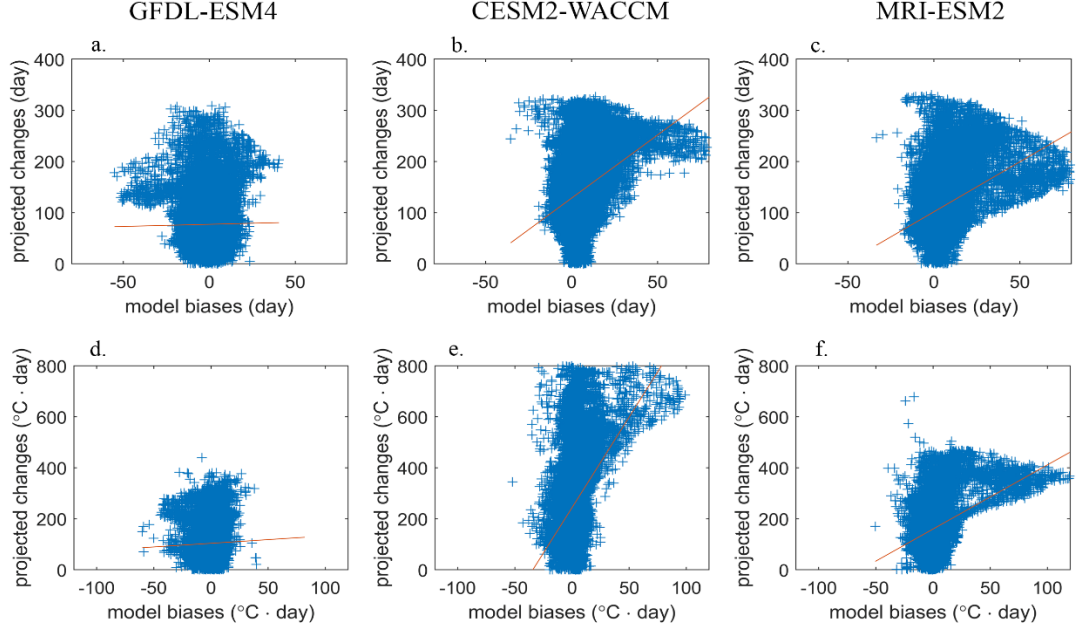
18

Figure 11. Historical model biases in warm-season MHW properties vs. the projected future changes over the global cells of kelp under SSP2-4.5 by the end of 21st century for the a.-c. the continuous warm-season MHW (D_c, day), d.-f. the accumulated heat stress over the continuous period (A_c, °C · day).

Over the coral and kelp cells, the pattern of future changes in the five thermal properties are similar to the changes globally, with increases across most cells in D_c, HS_{peak} and A_c as well as many decreases in HR_c and D_p, and higher magnitude of changes under the higher emission scenarios (Figure 8, 10; Table S1-6). The mean changes over the kelp cells are close to the global levels, while those over the coral cells are greater than the global averages in all three models (Table S1-6), in part because warm-water corals exist in the tropics and subtropics where the limited seasonality cause greater chance of continuous heat stress occurrence, and that contribute to higher accumulation of heat stress. For example, the mean level of D_c and A_c under SSP2-4.5 in GFDL-ESM4 is 178 day and 281 °C · day, respectively, while that across global ocean is 143 day and 246 °C · day (Figure 8; Table S1). For HS_{peak}, HR_c and D_p, however, the differences between the projected changes over the coral cells and the whole ocean varies among the models, ranging from negative to positive (Table S1-3). While it is unknown to what extent corals and kelp could adapt to recent thermal history in the future, the projected changes might be smaller if the thermal threshold increases due to acclimation and or adaptation. For example, the global mean increase in D_c by 2100 in the coral and kelp cells is 152 and 101 day shorter, respectively, using a thermal threshold based on the previous 60 years (2041-2100) rather than the historical period (Figure 8, 10).

Similar to the global patterns, the regional changes in these thermal properties also tend to be larger in CESM2-WACCM and MRI-ESM2 than those in GFDL-ESM4, which could be related to processes driving larger biases in those models (Figure 8, 10, S11-14). The projected increases of D_c and A_c across the coral and kelp cells show statistically significant positive relationships with the present-day model biases in each of those cells (Figure 9, 11, Table S7-12). The positive relationships, particularly for CESM2-WACCM and MRI-ESM2, indicates that coral and kelp cells with large positive biases are also exhibiting large projected changes in those same variables. This suggests that every 1 day increase in the model biases, for example in D_c, the projected values increase by 0.5, 1.2, 1.8 days in GFDL-ESM4, CESM2-WACCM and MRI-ESM2, respectively. However, the relationships between the projected changes and model biases for HS_{peak}, HR_c and D_p vary among the models with some of them not statistically significant (Table S7-12).

5. Discussion and conclusions

In this study, we evaluate the model biases in simulating five thermal properties of warm-season MHWs from three CMIP6 models, and analyze their potential role in the projected future changes with specific focus over the global regions of warm-water corals and kelp forests. By the end of 21st century, the duration, accumulated heat stress and peak intensity show systematic increases under all the future emission scenarios considered. Conversely, heating rate and the priming period display systematic decreases in the tropics and subtropics. The projected changes in warm-season MHW properties are broadly consistent in global patterns among the three models. However, there are regional disagreements on future MHW properties among the models as well as between present-day model simulations and the observations. Understanding the drivers of biases in the models is important in interpreting MHW projections and responsibly employing MHW projections in the studies of their ecological impacts. In the following section, we discuss the potential drivers of present-day model biases and the implications for future warm-season MHW projections.

The large model biases during the historical period and inter-model spread in the spatial pattern of the future projections are likely caused by different model representations of atmospheric and oceanic processes including 1) cloud formation; 2) deep convection, precipitation and storms, 3) surface winds and associated oceanic heat transport, and 4) ENSO dynamics. First, cloud representation in the tropics and subtropics help determine the peak intensity of MHWs by inducing anomalous radiation balance and surface heat flux that can cause anomalously warm SSTs. For example, the negative low cloud biases off the coast of California and Peru and in the Benguela current system lead to large warm bias in HS_{peak} observed in GFDL-ESM4 output (Dunne et al., 2020).

Second, heavy precipitation and storms may affect MHW duration, as associated strong winds and anomalous surface heat flux can cool the sea surface and terminate a MHW. Overestimated precipitation in parts of the tropical Pacific in GFDL-ESM4 due to Double Intertropical Convergence Zone (ITCZ) problem

could contribute to a shorter MHW duration than in the other two models (Danabasoglu et al., 2020; Dunne et al., 2020; Yukimoto et al., 2019). Tropical storms as well as deep convection associated with Madden Julian Oscillation (MJO) can also drive MHW dissolution; how accurately models simulate tropical storms and behaviors could therefore affect the simulation of MHW duration and the associated accumulated heat stress (Shin & Park, 2020).

Third, surface winds over the ocean influence SSTs and trigger anomalous heat stress at regional scales through affecting air-sea heat flux, wind-driven anomalous zonal advection and turbulent mixing (Bond et al., 2015; Sen Gupta et al., 2020; Holbrook et al., 2019; Oliver et al., 2017). In CESM2-WACCM, underestimated upwelling due to damped wind stress in the eastern boundary current regions could contribute to the positive biases in MHW duration off the west coasts of California, South Africa and South America (Danabasoglu et al., 2020). In GFDL-ESM4, the positive biases in the equatorial cyclonic wind stress and the negative biases in the zonal surface winds off the equator could enhance the surface heat loss at the equator and weaken surface heat loss off the equator by affecting vertical mixing of the warm surface later with cooler waters at depth (Dunne et al., 2020). This may partially explain the pattern of negative biases in MHW duration in the equatorial Pacific and more poleward positive biases. Shorter durations in the tropics in GFDL-ESM4 compared with the other models could also be driven by the shallower mixed layer in GFDL-ESM4, which would allow sea surface to warm or cool faster and stronger through air-sea heat flux. Faster and stronger warming due to the shoaled representation of the mixed layer depth might contribute to the higher peak temperatures (HS_{peak}) and larger rate of anomalous heat stress development (HR_{c}) in the tropics, relative to the other models.

Fourth, the inter-model variability in the thermal properties over the tropics are also related to model disagreements on the magnitude, location and timing of ENSO-driven SST anomalies. Though the simulations of ENSO dynamics have been improved with the latest generation of GCMs included in CMIP6, many uncertainties that can affect ENSO-driven heat stress remain (Beobide-Arsuaga et al., 2021; Brown et al., 2020; Jiang et al., 2021). Large warm biases for HS_{peak} in the eastern tropical Pacific by GFDL-ESM4 may be related to the underestimated convection in the western equatorial Pacific and stronger thermal stratification in the Pacific cold tongue region that could drive overestimated SSTs during ENSO events (Dunne et al., 2020). In contrast, there is no warm bias across the tropical Pacific in CESM2-WACCM and MRI-ESM2, which have improved representation of the stratocumulus clouds, and ocean mixing and stratification (Danabasoglu et al., 2020; Yukimoto et al., 2019).

Another fundamental source of model bias in simulating warm-season MHWs is the spatial resolution of the atmosphere and ocean components of the models. The spatial resolution of the atmospheric module in a GCM can affect many processes, notably cloud formation. Though this factor cannot explain the differences among the models we examined, as the models employed the

same resolution the atmosphere (Danabasoglu et al., 2020; Dunne et al., 2020; Yukimoto et al., 2019), it could influence the models' performance relative to observations. In addition, the spatial resolution of the ocean module in most GCMs is not fine enough to resolve small-scale processes, like boundary currents and mesoscale eddies, which may drive underestimates of heat stress which arise from variations in these oceanic processes. For example, in coastal and boundary current regions, underestimated magnitude of mesoscale eddies could lead to a negative heat stress bias due to its effects on heat transport (Guo et al., 2022; Hayashida et al., 2020; Oliver et al., 2019; Pilo et al., 2019), as shown in the negative biases of HS_{peak} in these regions across all models.

Coarse-spatial resolution can also cause unrealistically smooth SST time series due to high serial autocorrelation (Oliver et al., 2019), thereby leading to overestimated duration of continuous heat stress and underestimated duration of priming. The spatial resolution of GFDL-ESM4 is finer than that of CESM2-WACCM and MRI-ESM2 (Danabasoglu et al., 2020; Dunne et al., 2020; Yukimoto et al., 2019), which may partially explain the lower magnitude of model biases in GFDL-ESM4 and smaller coefficient of the relationship between historical model bias and projected change. While the resolution in the tropics and subtropics is similar among the models, the C-grid employed by GFDL-ESM4 could represent more realistic boundary features than the B-grid employed by the other two models; for example, the equatorial undercurrent could be represented up to twice as accurately using the C-grid as opposed to the B-grid at the same spatial resolution (Dunne et al., 2020). The positive biases for the duration and negative biases for peak intensity in most of the ocean by CESM2-WACCM and MRI-ESM2 might also be related to the limited spatial resolution of their ocean couplers. The systematic cold bias in the subpolar North Atlantic is known as a common error feature in GCMs due to the poor representation of mesoscale eddies (Danabasoglu et al., 2020; Dunne et al., 2020; Yukimoto et al., 2019).

Uncertainty in projected MHW properties may be larger in the tropics where SST can be more sensitive to model ability to simulate the aforementioned driving processes. In the tropics, a small positive bias in the mean state of SST could lead to large bias in the duration and accumulated heat stress due to the limited seasonality, which is reflected in the large positive biases for D_c and A_c in the tropical Pacific by CESM2-WACCM and MRI-ESM2. This is also shown in the large positive relationship between the future model projections and present-day model bias for D_c and A_c in the warm-water coral reef cells. Given this likely amplification of model bias, the future projections of the duration and accumulated heat stress, two metrics used for exploring ecological impacts of MHWs, need to be interpreted carefully in impacts modelling and research.

Future MHW studies can focus on examining the role of above driving processes using high resolution models with a large model ensemble of SST outputs, as it may advance the predictability of MHWs. Modelling experiments could be designed to examine the role of each of the physical processes which we identi-

fied might drive the model biases in simulating warm-season MHW properties. Given the essential contribution of high spatial resolution to the accuracy of MHW projections, future research characterizing MHW properties and their ecological impacts would benefit from using outputs from GCMs with finer ocean and atmospheric grids, although employing finer resolution SST output requires greater computational resources. Future work could also incorporate outputs from more GCMs and ESMs when data is available, considering the fact that this study is restricted in examining systematic biases for warm-season MHW properties due to the limited availability of daily SST model outputs. This would not only create a more robust ensemble of future projection, it would enable a more thorough analysis of the processes that systematically drive model biases in simulating MHWs. Meanwhile, including more ensemble member projections for each model may further constrain the uncertainties in terms of internal variability (e.g., ENSO) that could influence heat stress conditions.

It should be noted that the choice of thermal threshold for defining MHWs is fundamental to computing MHW projections and their ecological impacts. Most of the MHW projection studies to date used a fixed, historical thermal threshold to define MHWs (e.g., Hobday et al., 2016). As the ocean warms, marine organisms and ecosystems may adjust to a warmer baseline via physiological acclimatization, direction selection and changes in community structure, such that heat stress calculated from historical conditions is not representative. For example, there is evidence that coral reefs exposed to frequent heat stress may acquire higher thermal resistance (Hughes et al., 2018; Morikawa et al., 2019), though it may come with reduced coral diversity and structural complexity (Donner & Carilli, 2019; Magel et al., 2019). To better examine the projections of MHWs and their ecological impacts, more studies need to incorporate the role of acclimatization and adaptation into the definition of the heat stress baseline (Logan et al., 2014; McManus et al., 2020, 2021). We conducted a simple additional analysis here by quantifying MHWs relative to a rolling MMM threshold that represents theoretical adjustment to warming over time. Though the results are intuitive, the projection of less severe MHW properties assuming the rolling thermal threshold demonstrate the high sensitivity of MHW projections to the choice of threshold. This highlights the necessity of incorporating variable thermal thresholds, based on research into acclimation and adaptation in marine organisms and ecosystems (Alsuwaiyan et al., 2021), into future MHW projection and impact research.

With continued climate change and associated ocean warming, MHWs will continue to, or even more substantially, threaten marine ecosystems and the associated cultures, fisheries and incomes of local and Indigenous peoples (Cooley et al., 2022). To best understand the impact of increasing warm-season MHWs on marine organisms and ecosystems, we need to look beyond the accumulated intensity and examine the thermal properties like duration, heating rate and priming period. We also need to consider the ability of models to describe the processes driving MHW development and dissolution, as well as the extent to which organisms and ecosystems may adjust to warming. Considering these

factors, and the biases they may create in model output, is important for researchers studying the impact of MHWs on ecosystems. This cautious analysis of MHW projections is necessary to better inform policymakers and marine resource managers tasked with protecting marine life, and the people who depend on marine life, from the rising threat of MHWs.

Acknowledgments

Open Research

Datasets used in this study are all publicly available. The CMIP6 Global Daily 1° × 1° SST simulation outputs can be accessed at http://esgf-node.llnl.gov/search/cmip6/ and NOAA Coral Reef Watch CoralTemp v3.1 Global Daily 5 km SST dataset is available at https://coralreefwatch.noaa.gov/product/5km/index_5km_sst.php. The codes used to compute the warm-season marine heatwave metrics and produce the figures in the paper are available from the corresponding author upon request.

References

https://doi.org/10.34892/t2wk-5t34

Ainsworth, T. D., Heron, S. F., Ortiz, J. C., Mumby, P. J., Grech, A., Ogawa, D., et al. (2016). Climate change disables coral bleaching protection on the Great Barrier Reef. *Science*, *352*(6283), 338–342. https://doi.org/10.1126/science.aac7125Alsuwaiyan, N. A., Vranken, S., Filbee-Dexter, K., Cambridge, M., Coleman, M. A., & Wernberg, T. (2021). Genotypic variation in response to extreme events may facilitate kelp adaptation under future climates. *Marine Ecology Progress Series*, *672*, 111–121. https://doi.org/10.3354/MEPS13802Arafeh-Dalmau, N., Montaño-Moctezuma, G., Martinez, J. A., Beas-Luna, R., Schoeman, D. S., & Torres-Moye, G. (2019). Extreme Marine Heatwaves alter kelp forest community near its equatorward distribution limit. *Frontiers in Marine Science*, *6*(JUL), 499. https://doi.org/10.3389/fmars.2019.00499Arias-Ortiz, A., Serrano, O., Masqué, P., Lavery, P. S., Mueller, U., Kendrick, G. A., et al. (2018). A marine heatwave drives massive losses from the world's largest seagrass carbon stocks. *Nature Climate Change*, *8*(4), 338–344. https://doi.org/10.1038/s41558-018-0096-yBeobide-Arsuaga, G., Bayr, T., Reintges, A., & Latif, M. (2021).

Uncertainty of ENSO-amplitude projections in CMIP5 and CMIP6 models. *Climate Dynamics*, *56*(11–12), 3875–3888. https://doi.org/10.1007/s00382-021-05673-4Bond, N. A., Cronin, M. F., Freeland, H., & Mantua, N. (2015). Causes and impacts of the 2014 warm anomaly in the NE Pacific. *Geophysical Research Letters*, *42*(9), 3414–3420. https://doi.org/10.1002/2015GL063306Brown, J. R., Brierley, C. M., An, S. Il, Guarino, M. V., Stevenson, S., Williams, C. J. R., et al. (2020). Comparison of past and future simulations of ENSO in CMIP5/PMIP3 and CMIP6/PMIP4 models. *Climate of the Past*, *16*(5), 1777–1805. https://doi.org/10.5194/cp-16-1777-2020Cheung, W. W. L., Frölicher, T. L., Lam, V. W. Y., Oyinlola, M. A., Reygondeau, G., Rashid Sumaila, U., et al. (2021). Marine high temperature extremes amplify the impacts of climate change on fish and fisheries. *Science Advances*, *7*(40). https://doi.org/10.1126/sciadv.abh0895Cooley, S., Schoeman, D., Bopp, L., Boyd, P., Donner, S., Ito, S.-I., et al. (2022). Oceans and Coastal Ecosystems and their Services. In: Climate Change 2022: Impacts, Adaptation and Vulnerability. Contribution of Working Group II to the IPCC Sixth Assessment Report. *Cambridge University Press*, 20–22. Retrieved from https://www.ipcc.ch/report/ar6/wg1/#FullReportDanabasoglu, G., Lamarque, J. -F., Bacmeister, J., Bailey, D. A., DuVivier, A. K., Edwards, J., et al. (2020). The Community Earth System Model Version 2 (CESM2). *Journal of Advances in Modeling Earth Systems*, *12*(2), e2019MS001916. https://doi.org/10.1029/2019MS001916Donner, S. D., & Carilli, J. (2019). Resilience of Central Pacific reefs subject to frequent heat stress and human disturbance. *Scientific Reports*, *9*(1), 3484. https://doi.org/10.1038/s41598-019-40150-3Dunne, J. P., Horowitz, L. W., Adcroft, A. J., Ginoux, P., Held, I. M., John, J. G., et al. (2020). The GFDL Earth System Model Version 4.1 (GFDL-ESM 4.1): Overall Coupled Model Description and Simulation Characteristics. *Journal of Advances in Modeling Earth Systems*, *12*(11). https://doi.org/10.1029/2019MS002015Eyring, V., Bony, S., Meehl, G. A., Senior, C. A., Stevens, B., Stouffer, R. J., & Taylor, K. E. (2016). Overview of the Coupled Model Intercomparison Project Phase 6 (CMIP6) experimental design and organization. *Geoscientific Model Development*, *9*(5), 1937–1958. https://doi.org/10.5194/gmd-9-1937-2016Filbee-Dexter, K., Wernberg, T., Grace, S. P., Thormar, J., Fredriksen, S., Narvaez, C. N., et al. (2020). Marine heatwaves and the collapse of marginal North Atlantic kelp forests. *Scientific Reports*, *10*(1), 13388. https://doi.org/10.1038/s41598-020-70273-xFrölicher, T. L., Rodgers, K. B., Stock, C. A., & Cheung, W. W. L. (2016). Sources of uncertainties in 21st century projections of potential ocean ecosystem stressors. *Global Biogeochemical Cycles*, *30*(8), 1224–1243. https://doi.org/10.1002/2015GB005338Frölicher, T. L., Fischer, E. M., & Gruber, N. (2018). Marine heatwaves under global warming. *Nature*, *560*(7718), 360–364. https://doi.org/10.1038/s41586-018-0383-9Genin, A., Levy, L., Sharon, G., Raitsos, D. E., & Diamant, A. (2020). Rapid onsets of warming events trigger mass mortality of coral reef fish. *Proceedings of the National Academy of Sciences*, *117*(41), 25378–25385. https://doi.org/10.1073/pnas.2009748117Guo, X., Gao, Y., Zhang, S., Wu, L.,

Chang, P., Cai, W., et al. (2022). Threat by marine heatwaves to adaptive large marine ecosystems in an eddy-resolving model. *Nature Climate Change*, *12*(2), 179–186. https://doi.org/10.1038/s41558-021-01266-5Sen Gupta, A., Thomsen, M., Benthuysen, J. A., Hobday, A. J., Oliver, E., Alexander, L. V., et al. (2020). Drivers and impacts of the most extreme marine heatwaves events. *Scientific Reports*, *10*(1), 19359. https://doi.org/10.1038/s41598-020-75445-3Hayashida, H., Matear, R. J., Strutton, P. G., & Zhang, X. (2020). Insights into projected changes in marine heatwaves from a high-resolution ocean circulation model. *Nature Communications*, *11*(1), 4352. https://doi.org/10.1038/s41467-020-18241-xHilker, M., Schwachtje, J., Baier, M., Balazadeh, S., Bäurle, I., Geiselhardt, S., et al. (2016). Priming and memory of stress responses in organisms lacking a nervous system. *Biological Reviews*, *91*(4), 1118–1133. https://doi.org/10.1111/brv.12215Hobday, A. J., Alexander, L. V., Perkins, S. E., Smale, D. A., Straub, S. C., Oliver, E. C. J., et al. (2016). A hierarchical approach to defining marine heatwaves. *Progress in Oceanography*, *141*(8), 227–238. https://doi.org/10.1016/j.pocean.2015.12.014Hoeke, R. K., Jokiel, P. L., Buddemeier, R. W., & Brainard, R. E. (2011). Projected Changes to Growth and Mortality of Hawaiian Corals over the Next 100 Years. *PLoS ONE*, *6*(3), e18038. https://doi.org/10.1371/journal.pone.0018038Holbrook, N. J., Scannell, H. A., Sen Gupta, A., Benthuysen, J. A., Feng, M., Oliver, E. C. J., et al. (2019). A global assessment of marine heatwaves and their drivers. *Nature Communications*, *10*(1), 2624. https://doi.org/10.1038/s41467-019-10206-zVan Hooidonk, R., & Huber, M. (2012). Effects of modeled tropical sea surface temperature variability on coral reef bleaching predictions. *Coral Reefs*, *31*(1), 121–131. https://doi.org/10.1007/s00338-011-0825-4Hughes, T. P., Kerry, J. T., Álvarez-Noriega, M., Álvarez-Romero, J. G., Anderson, K. D., Baird, A. H., et al. (2017). Global warming and recurrent mass bleaching of corals. *Nature*, *543*(7645), 373–377. https://doi.org/10.1038/nature21707Hughes, T. P., Kerry, J. T., Baird, A. H., Connolly, S. R., Dietzel, A., Eakin, C. M., et al. (2018). Global warming transforms coral reef assemblages. *Nature*, *556*(7702), 492–496. https://doi.org/10.1038/s41586-018-0041-2Jayathilake, D. R. M., & Costello, M. J. (2020). A modelled global distribution of the kelp biome. *Biological Conservation*, *252*, 108815. https://doi.org/10.1016/J.BIOCON.2020.108815Jiang, W., Huang, P., Huang, G., & Ying, J. (2021). Origins of the excessive westward extension of ENSO SST simulated in CMIP5 and CMIP6 models. *Journal of Climate*, *34*(8), 2839–2851. https://doi.org/10.1175/JCLI-D-20-0551.1Jones, P. W. (1999). First- and Second-Order Conservative Remapping Schemes for Grids in Spherical Coordinates. *Monthly Weather Review*, *127*(9), 2204–2210. https://doi.org/10.1175/1520-0493(1999)127<2204:FASOCR>2.0.CO;2Li, G., & Xie, S. P. (2012). Origins of tropical-wide SST biases in CMIP multi-model ensembles. *Geophysical Research Letters*, *39*(22), n/a-n/a. https://doi.org/10.1029/2012GL053777Li, X., & Donner, S. D. (2022). Lengthening of warm periods increased the intensity of warm-season marine heatwaves over the past 4 decades. *Climate Dynamics*, *1*, 3. https://doi.org/10.1007/s00382-022-06227-yLogan, C. A., Dunne, J. P., Eakin, C. M., & Donner, S. D. (2014). Incorporating adaptive responses into

future projections of coral bleaching. *Global Change Biology*, *20*(1), 125–139. https://doi.org/10.1111/gcb.12390Magel, J. M. T., Burns, J. H. R., Gates, R. D., & Baum, J. K. (2019). Effects of bleaching-associated mass coral mortality on reef structural complexity across a gradient of local disturbance. *Scientific Reports 2019 9:1*, *9*(1), 1–12. https://doi.org/10.1038/s41598-018-37713-1McManus, L. C., Vasconcelos, V. V., Levin, S. A., Thompson, D. M., Kleypas, J. A., Castruccio, F. S., et al. (2020). Extreme temperature events will drive coral decline in the Coral Triangle. *Global Change Biology*, *26*(4), 2120–2133. https://doi.org/10.1111/GCB.14972McManus, L. C., Forrest, D. L., Tekwa, E. W., Schindler, D. E., Colton, M. A., Webster, M. M., et al. (2021). Evolution and connectivity influence the persistence and recovery of coral reefs under climate change in the Caribbean, Southwest Pacific, and Coral Triangle. *Glob Change Biol*, *27*, 4307–4321. https://doi.org/10.1111/gcb.15725Morikawa, M. K., Palumbi, S. R., Baker, A. C., Kaufman, L., & Knowlton, N. (2019). Using naturally occurring climate resilient corals to construct bleaching-resistant nurseries. *Proceedings of the National Academy of Sciences of the United States of America*, *116*(21), 10586–10591. https://doi.org/10.1073/PNAS.1721415116O'neill, B. C., Tebaldi, C., Van Vuuren, D. P., Eyring, V., Friedlingstein, P., Hurtt, G., et al. (2016). The Scenario Model Intercomparison Project (ScenarioMIP) for CMIP6. *Geosci. Model Dev*, *9*, 3461–3482. https://doi.org/10.5194/gmd-9-3461-2016Oliver, E. C. J., Benthuysen, J. A., Bindoff, N. L., Hobday, A. J., Holbrook, N. J., Mundy, C. N., & Perkins-Kirkpatrick, S. E. (2017). The unprecedented 2015/16 Tasman Sea marine heatwave. *Nature Communications*, *8*, 16101. https://doi.org/10.1038/ncomms16101Oliver, E. C. J., Donat, M. G., Burrows, M. T., Moore, P. J., Smale, D. A., Alexander, L. V., et al. (2018). Longer and more frequent marine heatwaves over the past century. *Nature Communications*, *9*(1), 1324. https://doi.org/10.1038/s41467-018-03732-9Oliver, E. C. J., Burrows, M. T., Donat, M. G., Sen Gupta, A., Alexander, L. V., Perkins-Kirkpatrick, S. E., et al. (2019). Projected Marine Heatwaves in the 21st Century and the Potential for Ecological Impact. *Frontiers in Marine Science*, *6*, 734. https://doi.org/10.3389/fmars.2019.00734Pilo, G. S., Holbrook, N. J., Kiss, A. E., & Hogg, A. M. C. (2019). Sensitivity of Marine Heatwave Metrics to Ocean Model Resolution. *Geophysical Research Letters*, *46*(24), 14604–14612. https://doi.org/10.1029/2019GL084928Plecha, S. M., Soares, P. M. M., Silva-Fernandes, S. M., & Cabos, W. (2021). On the uncertainty of future projections of Marine Heatwave events in the North Atlantic Ocean. *Climate Dynamics*, *56*(7–8), 2027–2056. https://doi.org/10.1007/s00382-020-05529-3Rogers-Bennett, L., & Catton, C. A. (2019). Marine heat wave and multiple stressors tip bull kelp forest to sea urchin barrens. *Scientific Reports*, *9*(1), 15050. https://doi.org/10.1038/s41598-019-51114-yShin, J., & Park, S. (2020). Impacts of ENSO and Madden–Julian oscillation on the genesis of tropical cyclones simulated by general circulation models and compared to observations. *Environmental Research Letters*, *15*(3), 034046. https://doi.org/10.1088/1748-9326/ab7466Skirving, W., Marsh, B., De La Cour, J., Liu, G., Harris, A., Maturi, E., et al. (2020). Coraltemp and the coral

reef watch coral bleaching heat stress product suite version 3.1. *Remote Sensing*, *12*(23), 1–10. https://doi.org/10.3390/rs12233856Skirving, W. J., Heron, S. F., Marsh, B. L., Liu, G., De La Cour, J. L., Geiger, E. F., & Eakin, C. M. (2019). The relentless march of mass coral bleaching: a global perspective of changing heat stress. *Coral Reefs*, *38*(4), 547–557. https://doi.org/10.1007/s00338-019-01799-4Smale, D. A. (2020). Impacts of ocean warming on kelp forest ecosystems. *New Phytologist.* https://doi.org/10.1111/nph.16107Smale, D. A., Wernberg, T., Oliver, E. C. J., Thomsen, M., Harvey, B. P., Straub, S. C., et al. (2019, April 4). Marine heatwaves threaten global biodiversity and the provision of ecosystem services. *Nature Climate Change.* Nature Publishing Group. https://doi.org/10.1038/s41558-019-0412-1Sully, S., Burkepile, D. E., Donovan, M. K., Hodgson, G., & van Woesik, R. (2019). A global analysis of coral bleaching over the past two decades. *Nature Communications*, *10*(1). https://doi.org/10.1038/s41467-019-09238-2Toniazzo, T., & Woolnough, S. (2014). Development of warm SST errors in the southern tropical Atlantic in CMIP5 decadal hindcasts. *Climate Dynamics*, *43*(11), 2889–2913. https://doi.org/10.1007/s00382-013-1691-2UNEP-WCMC, World-Fish Centre, WRI, TNC (2021). Global distribution of warm-water coral reefs, compiled from multiple sources including the Millennium Coral Reef Mapping Project. Version 4.1. Includes contributions from IMaRS-USF and IRD (2005), IMaRS-USF (2005) and Spalding et al. (2001). Cambridge (UK): UN Environment World Conservation Monitoring Centre. Data DOI: Wang, C., Zhang, L., Lee, S.-K., Wu, L., & Mechoso, C. R. (2014). A global perspective on CMIP5 climate model biases. *Nature Climate Change*, *4*(3), 201–205. https://doi.org/10.1038/nclimate2118Weigel, A. P., Knutti, R., Liniger, M. A., & Appenzeller, C. (2010). Risks of Model Weighting in Multimodel Climate Projections. *Journal of Climate*, *23*(15), 4175–4191. https://doi.org/10.1175/2010JCLI3594.1Yukimoto, S., Kawai, H., Koshiro, T., Oshima, N., Yoshida, K., Urakawa, S., et al. (2019). The meteorological research institute Earth system model version 2.0, MRI-ESM2.0: Description and basic evaluation of the physical component. *Journal of the Meteorological Society of Japan*, *97*(5), 931–965. https://doi.org/10.2151/jmsj.2019-051